Molecular Therapy
Nucleic Acids
Original Article

Expanding DdCBE-mediated targeting scope to aC motif preference in rat

Xiaolong Qi,[1,10] Lei Tan,[2,10] Xu Zhang,[1,10] Jiachuan Jin,[3,10] Weining Kong,[1,10] Wei Chen,[1,10] Jianying Wang,[2] Wei Dong,[1] Lijuan Gao,[1] Lijun Luo,[1] Dan Lu,[1] Jianan Gong,[1] Feifei Guan,[1] Wenjie Shu,[4] Xingxu Huang,[5] Lianfeng Zhang,[1,6] Shengqi Wang,[4] Bin Shen,[2,5,7,8] and Yuanwu Ma[1,6,9]

[1]Key Laboratory of Human Disease Comparative Medicine, National Health Commission of China (NHC), Beijing Engineering Research Center for Experimental Animal Models of Human Critical Diseases, Institute of Laboratory Animal Science, Chinese Academy of Medical Sciences, Peking Union Medicine College, Beijing 100021, China; [2]State Key Laboratory of Reproductive Medicine, Women's Hospital of Nanjing Medical University, Nanjing Maternity and Child Health Care Hospital, Nanjing Medical University, Nanjing, Jiangsu 211100, China; [3]Center for Reproductive Medicine, The Third Affiliated Hospital of Zhengzhou University, Zhengzhou 450052, China; [4]Bioinformatics Center of AMMS, Beijing 100850, China; [5]Zhejiang Laboratory, Hangzhou, Zhejiang 311121, China; [6]Neuroscience Center, Chinese Academy of Medical Sciences, Beijing 100730, China; [7]Gusu School, Nanjing Medical University, Nanjing, Jiangsu 215031, China; [8]Center for Global Health, School of Public Health, Nanjing Medical University, Nanjing, Jiangsu 211100, China; [9]National Human Diseases Animal Model Resource Center, Institute of Laboratory Animal Science, Chinese Academy of Medical Sciences, Peking Union Medicine College, Beijing 100021, China

An animal model harboring pathogenic mitochondrial DNA (mtDNA) mutations is important to understand the biological links between mtDNA variation and mitochondrial diseases. DdCBE, a DddA-derived cytosine base editor, has been utilized in zebrafish, mice, and rats for tC sequence-context targeting and human mitochondrial disease modeling. However, human pathogenic mtDNA mutations other than the tC context cannot be manipulated. Here, we screened the combination of different DdCBE pairs at pathogenic mtDNA mutation sites with nC (n for a, g, or c) context and identified that the left-G1333C (L1333C) + right G1333N (R1333N) pair could mediate C•G-to-T•A conversion effectively at aC sites in rat C6 cells. The editing efficiency at disease-associated mtDNA mutation sites within aC context was further confirmed to be up to 67.89% *in vivo*. Also, the installed disease-associated mtDNA mutations were germline transmittable. Moreover, the edited rats showed impaired cardiac function and mitochondrial function, resembling human mitochondrial disease symptoms. In summary, for the first time, we expanded the DdCBE targeting scope to an aC motif and installed the pathogenic mutation in rats to model human mitochondrial diseases.

INTRODUCTION

In animal cells, mitochondria are the only organelles containing their genome, mitochondrial DNA (mtDNA). mtDNA mutations are closely related to a broad spectrum of diseases. More than 387 pathogenic variants of mtDNA in humans have been reported (www.mitomap.org). No curative treatments are currently available for patients with mtDNA mutations. Genetically mtDNA-modified animal models are urgently needed to advance our understanding of the physiopathology of mitochondrial diseases and to develop therapeutic approaches. Due to mtDNA resistance to transgenic manipulation, only a handful of genetically gene-modified animal models are available.[1]

In 2020, a breakthrough technology named DdCBE paved the way to produce an animal model with desired mtDNA mutations at tC sites. Given the advantages of this tool, we generated zebrafish and rats containing desired mtDNA mutations to resemble human mitochondrial diseases.[2,3] However, due to the strict tC sequence-context constraint of DddA, human pathogenic mtDNA mutations without the tC context cannot be edited. In addition, mutation with the tC context only accounts for a small part of mtDNA pathogenic mutations (46/387). Hence, the strategy is urgently needed to expand the DdCBE targeting scope to non-tC sites. Recently, Mok et al. applied phage-assisted continuous and non-continuous evolution strategies to increase DdCBE activity at both tC and non-tC targets. The evolved DdCBE can improve the mtDNA editing efficiency and broaden the targeting scope.[4] However, compared with the canonical version, the evolved ones induce more bystander mutations in spacing regions and lose the ability to precisely edit a specific single base.

Received 6 October 2022; accepted 22 February 2023;
https://doi.org/10.1016/j.omtn.2023.02.028.

[10]These authors contribute equally

Correspondence: Shengqi Wang, Bioinformatics Center of AMMS, Beijing 100850, China.
E-mail: sqwang@bmi.ac.cn
Correspondence: Bin Shen, State Key Laboratory of Reproductive Medicine, Women's Hospital of Nanjing Medical University, Nanjing Maternity and Child Health Care Hospital, Nanjing Medical University, Nanjing, Jiangsu 211100, China.
E-mail: binshen@njmu.edu.cn
Correspondence: Yuanwu Ma, Key Laboratory of Human Disease Comparative Medicine, National Health Commission of China (NHC), Beijing Engineering Research Center for Experimental Animal Models of Human Critical Diseases, Institute of Laboratory Animal Science, Chinese Academy of Medical Sciences, Peking Union Medicine College, Beijing 100021, China.
E-mail: mayuanwu@cnilas.org

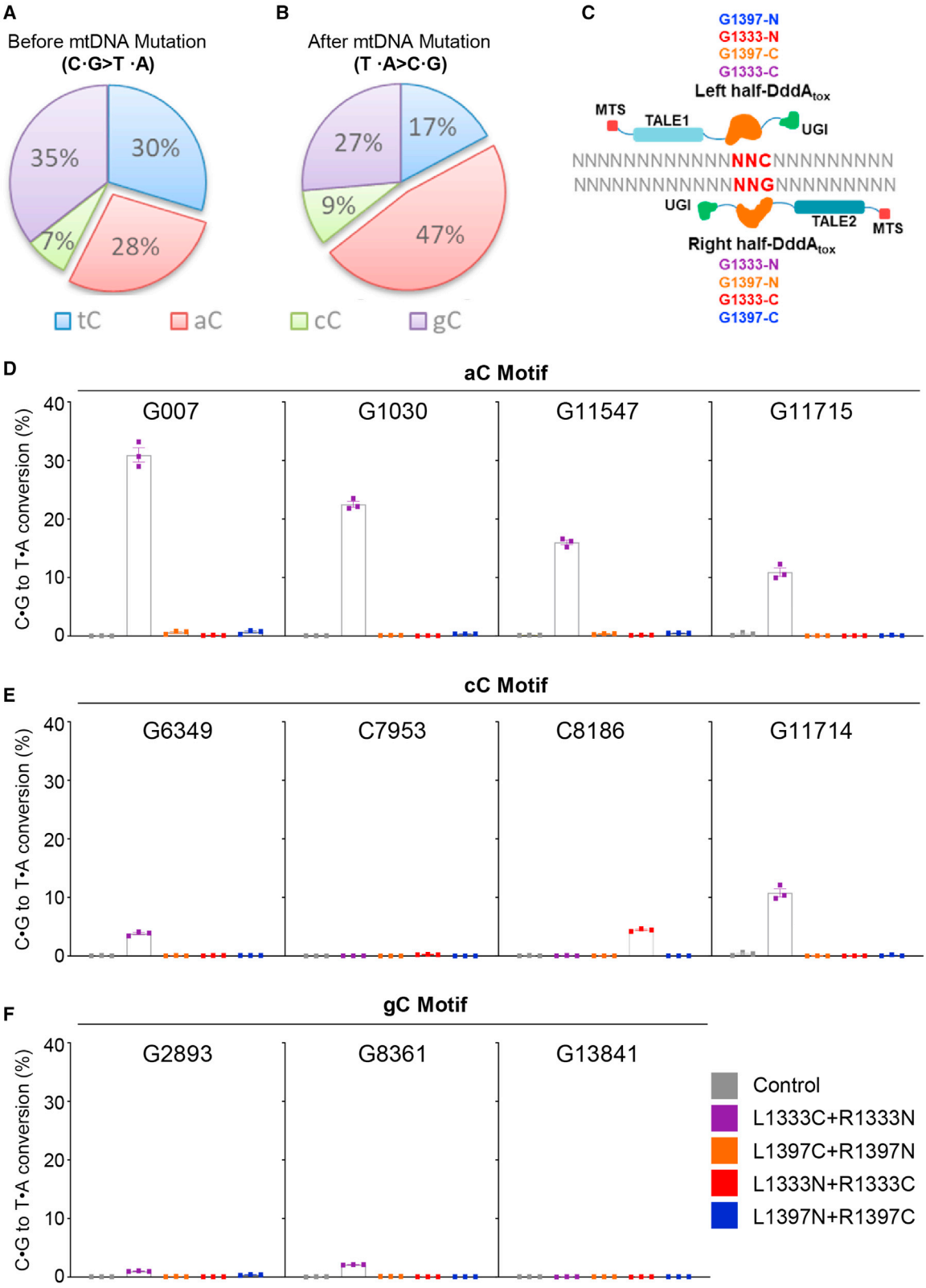

(legend on next page)

Here, we analyzed all reported human pathogenic mtDNA mutation sites with C•G-to-T•A conversion and screened the editing efficiency at conserved pathogenic mtDNA mutations with nC (n for a, g, or c) context using different combined DdCBE pairs in rat glioma C6 cells. We identified that the canonical DdCBE pair with the left-G1333C (L1333C) + right G1333N (R1333N) combination mediates C•G-to-T•A conversion at aC sites with high editing preference and low bystander editing effects. Encouraged by this finding, we injected the proven DdCBE pair into one-cell zygotes and successfully obtained rats harboring desired mtDNA mutations at aC sites with frequencies up to 67.89%. We further demonstrated that the installed disease-associated mtDNA mutations were germline transmittable, and the edited rats could resemble human mitochondrial disease symptoms. We also performed off-target analyses and revealed that our selected DdCBE pairs targeting aC sites enabled precise base editing with limited off-target effects in rat.

RESULTS

Expanding the DdCBE targeting scope

We analyzed all reported human pathogenic mtDNA mutations and found that only 30% (46/155) of C•G-to-T•A conversion at the tC motif might be edited to model human mitochondrial disease (Figure 1A; Table S1) and 17% (28/163) of the tC motif formed after T•A-to-C•G conversion might be corrected by DdCBE (Figure 1B; Table S1). To expand the DdCBE targeting scope, non-tC sites conserved between human and rat were selected to test different combined DdCBE pairs' activity. Four DdCBE pairs (L1333C + R1333N, L1397C + R1397N, L1333N + R1333C, and L1397N + R1397C) were designed for each target site (Figure 1C), and the C•G-to-T•A conversion efficiency at these sites was evaluated in rat glioma C6 cells. The DdCBE expression plasmids were assembled by the Golden Gate strategy as described before.[2,3] Rat G007, G1030, G11547, and G11715 sites with a conserved aC motif between human and rat, corresponding to human G583, G1606, G12147, and G12316 sites, respectively(Figure S1A–S1D), were randomly selected for aC motif-based DdCBE targeting. The Sanger sequencing (Figure S1I) and deep sequencing (Figure 1D) results indicated that the L1333C + R1333N pair showed high editing activity at aC sites. The mutation loads at the G007, G1030, G11547, and G11715 sites were up to 30.94% ± 1.22%, 22.50% ± 0.50%, 15.99% ± 0.72%, and 10.77% ± 0.69%, respectively. The rat G6349, G7953, G8186, and G11714 sites, corresponding to human G6930, G8561, G8794, and G12315 sites, respectively (Figures S1D and S2A–S2C), were selected for cC motif-based DdCBE targeting. The deep sequencing (Figure 1E) data showed that the L1333C + R1333N pair had editing activity at the G6349 and G11714 sites with frequencies of 3.8% ± 0.35% and 10.93% ± 0.71%, respectively, and the L1333N + R1333C pair was observed with low editing activity at the G8186 site with frequencies of 4.42% ± 0.22% (Figure 1E). The rat G2893, G8361, and G13841 sites, corresponding to human G3460, G8969, and G14453 sites, respectively (Figures S3A–S3C), were selected for gC motif-based DdCBE targeting. The deep sequencing (Figure 1F) data indicated that all DdCBE pairs showed inefficient editing activity. These results suggested that the L1333C + R1333N pair displayed a strong preference for aC context while showing no obvious bystander editing around the target sites (Figures S1E–S1H). Interestingly, although the G11714 site possesses an acC context, it could be edited with the G11715 site simultaneously by the same L1333C + R1333N pair (Figures S1H and S1I). This phenomenon was also observed for C within a tcC context, which also could be edited efficiently by DdCBE.[3] Taken together, our results demonstrate that the DdCBE pair (L1333C + R1333N) can mediate mtDNA C•G-to-T•A conversion with a high editing preference at aC sites.

DdCBE-mediated mtDNA editing at the aC motif in rats

To further validate the established DdCBE pair editing efficiency *in vivo*, we selected three conserved aC/aCC sites to mimic human pathogenic mutations G583A, G1606A, and G12315/6A. The G583A mutation in mtDNA *Trnf* ($tRNA^{Phe}$) is linked to asymptomatic retinopathy and mitochondrial myopathy in humans.[5,6] The G1606A mutation in mtDNA *Trnv* ($tRNA^{Val}$) is associated with a characteristic complex neurological phenotype.[7,8] The G12315/6A mutations in the mtDNA *Trnl2* ($tRNA^{Leu\ (CUN)}$) gene are related to atherosclerotic lesions and muscle degeneration-associated syndrome.[9,10] The DdCBE expression plasmids were purified and directly injected into rat fertilized eggs for mtDNA editing as described previously.[3] For the G007 site, 5 out of 25 pups were successfully edited, with frequencies of 33.22%–67.89% (Figures 2A and 2D; Table 1). For the G1030 site, 3 out of 12 pups were edited with frequencies of 7.28%–24.1% (Figures 2B and 2E; Table 1). For the G11714/5 sites, 4 out of 11 pups were edited with frequencies that ranged from 19.11% to 40.68% (Figures 2C and 2F; Table 1). Within the spacing region, no more than 0.02% bystander editing was detected for the G007-DdCBE (Figure 2D) and G11714/5-DdCBE pairs (Figure 2F), and no more than 1% bystander editing was detected for G1030-DdCBE pair (Figure 2E).

A primer pair was designed to detect the random insertion of DdCBE in the rat genome. Although it has been reported that direct injection of circular plasmids could minimize random genome insertion,[11] transgenesis was also detected in #2 and #9 of G007A F_0 rats (Figure S4A), #7 and #8 of G1030A F_0 rats (Figure S4B), and #2 and #10 from G11714/5A F_0 rats (Figure S4C). The DdCBE insertion would not yield a higher mtDNA editing efficiency (Figures 2D–2F). To characterize the mutation loads among various tissues, G007A F_0-#2 (Figure S4D and S4G), G1030A F_0-#12 (Figures S4E

Figure 1. Screening of DdCBE pairs targeting non-tC motifs in rat C6 cells

(A) The percentage of gC, tC, aC, and cC motifs of reference loci corresponding to the reported human mtDNA C·G-to-T·A mutations (data collected from MitoMap Database). (B) The percentage of 4 motifs of reported human mtDNA T·A-to-C·G mutations. (C) Schematic overview of the four DdCBE pair combinations used in this study. (D–F) The rat mtDNA sites with aC motif (D), cC motif (E), and gC motif (F) were selected to test the DdCBE-mediated conversion efficiency in rat C6 cells. (D–F) Data are represented as mean ± SEM.

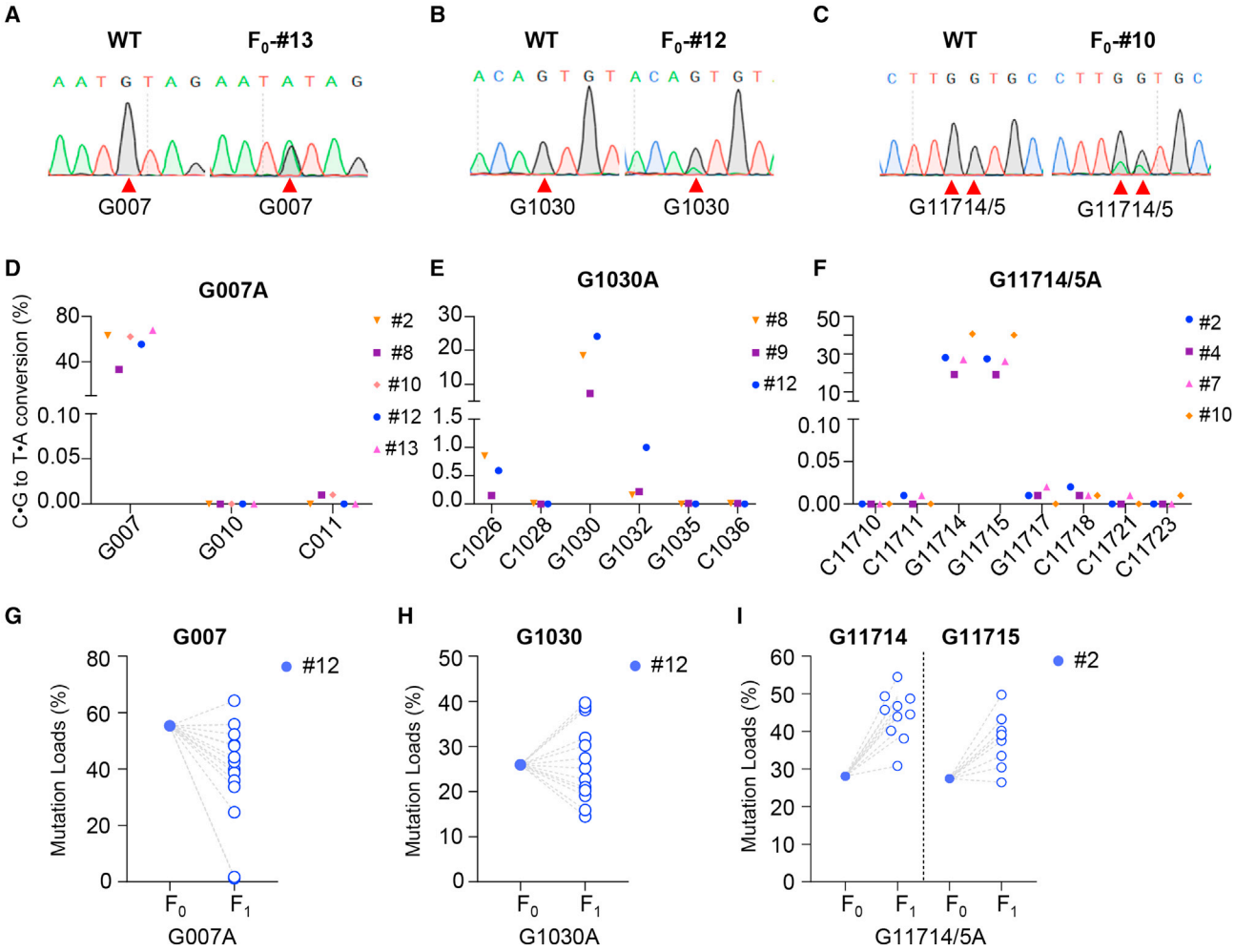

Figure 2. DdCBE-mediated mtDNA editing at aC motif in rats

(A–C) Sanger sequencing chromatograms of mtDNA G007 (A), G1030 (B), and G11714/5 (C) sites in wild-type and edited rats. (D–F) Frequencies of G-to-A conversion within the spacing region in G007A (D), G1030A (E), and G11714/5A (F) F_0 rats. (G–I) The mutation loads in G007A F_1 rats (G), G1030A F_1 rats (H), and G11714/5A F_1 rats (I).

and S4H), and G11714/5A F_0-#2 (Figures S4F and S4I) were sacrificed to collect tissues for Sanger sequencing and deep sequencing. The results showed that mtDNA editing efficiencies among different tissues were comparable (Figure S4D–S4I). Together, our well-proven DdCBE combination pair works well to mediate mtDNA editing at aC sites in rats.

DdCBE-mediated mtDNA editing in rat is heritable

The female rats of G007A F_0-#12, G1030A F_0-#12, and G11714/5A F_0-#2 were crossed with wild-type males for germline-transmission tests. As a result, 14 out of 16 F_1 pups generated from the G007A founder were detected with the expected mutation by Sanger sequencing (Figure 2G; Table S2). For G1030A, all offspring from the F_0 rat were also detected with targeted mutations (Figure 2H; Table S2). For G11714/5A, the targeted mutations were detected in all F_1 pups (Figure 2I; Table S2). Consistent with our previous data,[3] offspring harbored variable mutation loads. Some pups showed higher mutation loads, while others showed lower mutation loads, compared with mother (Figures 2G–2I). We also performed Sanger sequencing and deep sequencing in 9 tissues of F_1 offspring. The results showed that the mutation loads were comparable among various tissues (Figure S5A–S5F). These results demonstrate that DdCBE-mediated mtDNA editing at aC sites can be transmitted to the next generation.

G007A mutant rats exhibit dilated cardiomyopathy

In human, mtDNA G583 is located in the stem region of the tRNA for phenylalanine, and its mutation is associated with mitochondrial myopathy.[6] The G007A F_0-#13 rat harbored high mutation loads in toe (Figures 2A and 2D) and looked weaker than its littermate; it was then sacrificed to analyze mutation loads and pathological changes in muscle and heart. The Sanger sequencing and deep sequencing results showed that it harbored high mutation loads in skeletal muscle and heart tissues, as that in toe (Figures 3A and

Table 1. Injection summary of DdCBE-mediated rat mtDNA editing

Target site	Con. (ng/μL)	No. of injected zygotes	No. of transplanted zygotes	No. of pups	No. of edited pups	Mutation loads (%)
G007	7 + 7	84	59	25	5	33.22–67.89
G1030	7 + 7	90	51	12	3	7.28–24.1
G11714/5	7 + 7	159	96	11	4	19.11–40.68

3B). We observed disrupted muscle fibers in skeletal muscle and heart using hematoxylin and eosin (H&E) staining (Figure 3C). Further, we used transmission electron microscopy (TEM) to examine the mitochondrial morphology and ultrastructure. Dilated mitochondria and evident cristae degeneration in the mitochondrial matrix were observed both in the skeletal muscle and heart of the G007A F_0-#13 rat (Figure 3D). We observed that the ATP level in G007A F_0-#13 skeletal muscle and heart tissue decreased significantly (Figure S6A). Additionally, mitochondrial proteins were all down-regulated either encoded by the nuclear or mitochondrial genome (Figure 3E). We also analyzed the transcription changes and copy number of mtDNA in heart and muscle of G007A F_0 mutant rats. We observed that all 13 transcriptions of mitochondrial protein-coding genes were significantly upregulated (Figure S7A–S7D) and that mtDNA copy numbers increased (Figure S7E–S7H).

Encouraged by the findings in the G007A F_0-#13 rat, we analyzed the cardiac structure and function of G007A F_1 rats at 6 weeks of age. The results showed that G007A F_1 rats exhibited dilated cardiomyopathy (DCM) phenotypes with larger chambers and decreased contraction (Figure 3F). These changes were further confirmed by increased left ventricular (LV) diameter at the end of systole and diastole (LVIDS and LVIDD, respectively) (Figures 3G and 3H), increased LV volume at the end of systole and diastole (LVVS and LVVD, respectively) (Figures 3I and 3J), decreased LV ejection fraction (LVEF) (Figure 3K), and no obvious changes in fractional shortening (LVFS), LV anterior wall at the end of systole and distole (LVAWS and LVAWD), LV posterior wall at the end of systole and diastole (LVPWS and LVPWD) (Figure S6B–S6F). Then, we analyzed the motor ability of G007A F_1 rats and found that their moved distance and speed decreased significantly (Figures 3L and S6G). These results suggest that rats with G007A mutation could reproduce the phenotype of human mitochondrial disease.

G11714/5A mutant rats exhibit hypertrophic cardiomyopathy

In human, G12315/6 is located in the TΨC arms of tRNA for leucine, and its mutation is clinically associated with limb and respiratory muscle weakness and degeneration.[12,13] In G11714/5A F_1 rats, although we did not observe a significant reduction in their motor ability (Figures S8A and S8B), we unexpectedly found that these pups exhibited a hypertrophic cardiomyopathy (HCM) phenotype at 8 weeks of age, with smaller chambers and enhanced cardiac contractility (Figure 4A). These characteristics were further demonstrated by decreased LVIDS (Figure 4B), decreased LVVD and LVVS (Figures 4C and 4D), increased LVEF and LVFS (Figures 4E and 4F), and increased LVAWS, LVAWD, and LVPWS (Figures 4G–4I). There is no case report showing that patients with G12315A or G12316A mutations could develop HCM. Our distinct phenotype observed in G11714/5A rats might be account for two adjacent G base conversions, suggesting that two adjacent G mutations in G12315/6 may be a risk factor of HCM.

Off-target effect of DdCBE

To profile the off-target effect of DdCBE, we performed whole mtDNA sequencing and nuclear DNA targeted deep sequencing in the edited F_0 rats and F_1 rats for each target site.

Compared with the wild-type control, there were sparse off-target events along the whole mitochondrial genome in the edited F_0 rats (Figure 5A). To further evaluate the off-target effects induced by DdCBE, off-target sites (OTSs) with conversion rates over 1% were further analyzed. There were 5 OTSs for G007-DdCBE (Figures 5B), 1 OTS for G1030-DdCBE (Figure 5C), and 4 OTSs for G11714/5-DdCBE (Figure 5D). Among the 10 OTSs, eight sites were detected with a tC motif, and two sites were detected with an aC motif, suggesting that DdCBE could edit aC sites at both on-target sites and OTSs. Although C14351T, located on *Cytb* gene, is a synonymous mutation, up to 25.01% of off-target editing in G1030A founders still caught our attention (Figure 5C). By aligning the TALE recognition sequence against the whole mitochondrial genome, we found that the C14351T mutation may be induced by the sequence-dependent activity of G1030-DdCBE (Figure S9A). The average frequencies of mitochondrial genome-wide off-target editing by G11714/5-DdCBE were similar to these of wild-type rats, whereas G007-DdCBE and G1030-DdCBE showed slightly higher off-target editing frequencies (Figure 5E). These results demonstrate that our established DdCBE pair could mediate precise base editing within the aC context in the rat mitochondrial genome with limited off-target effects.

To analyze the potential off-target editing in the rat nuclear genome induced by DdCBE, putative OTSs with identical sequences to each TALE binding site of rG007A-, rG1030A-, and rG11714/5-DdCBEs were selected. For rG007A-DdCBE, six potential OTSs (OTS1–OTS6) with sequence similarity to the rG007A L-TALE-binding site and two potential OTSs (OTS7, OTS8) for rG007A R-TALE were obtained (Figure S10A). For rG1030A-DdCBE, only two potential OTSs (OTS1 and OTS2) for rG1030A R-TALE were obtained (Figure S11A). For rG11714/5-DdCBE, two potential OTS (OTS1 and OTS2) for rG11714/15A L-TALE and five potential OTSs

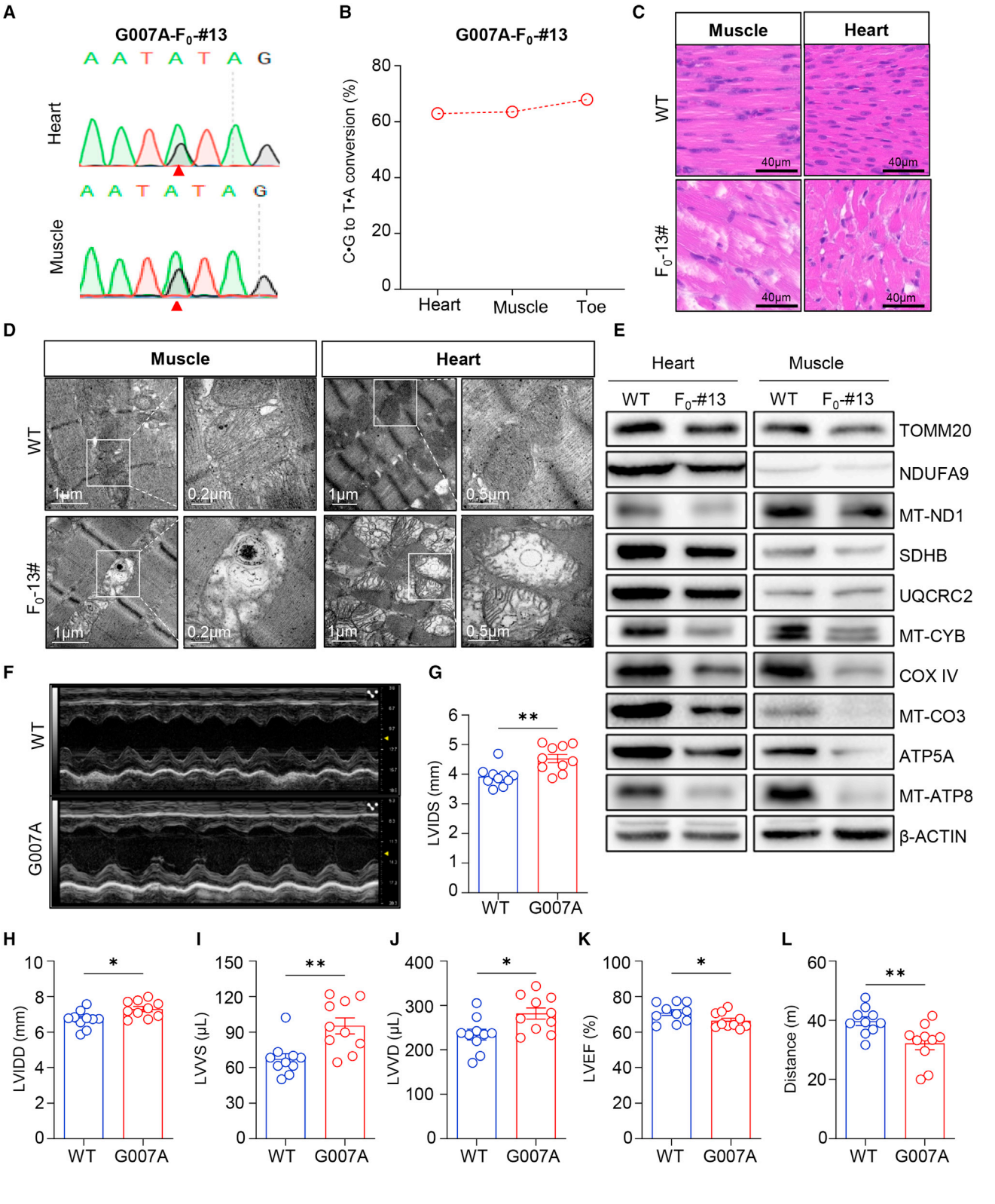

(legend on next page)

(OTS3–OTS7) for rG11714/15A R-TALE were found (Figure S12A). Among them, one potential OTS (OTS8) had an identical sequence to both TALE binding sites of rG11714/5-DdCBEs. Then, we analyzed the editing events at these potential OTSs in heart, muscle, brain, and ear of G007A rats (F_0-#2, F_1-#11, F_1-#15, and F_1-#17), G1030A rat (F_0-#12), and G11714/5A rats (F_0-#2, F_1-#20, F_1-#21, and F_1-#22) using targeted deep sequencing. The results showed that no detectable off-target editing events were detected in the edited rats (Figure S10B, S11B, and S12B).

DISCUSSION

In this study, for the first time, we identified a particular combination of the DdCBE split (L1333C + R1333N) with an aC site targeting preference in rat C6 cells. Using the identified DdCBE combination pair, we successfully induced C•G-to-T•A conversion in rat G007, G1030, and G11714/5 loci with an efficiency of 20% (5/25), 25% (3/12), and 36% (4/11), respectively. The highest mutation load was up to 67.89%. The edited female F_0 rats were crossed with wild-type Sprague Dawley (SD) rats, and the F_1 offspring showed detectable mutation loads as expected. Interestingly, offspring harbored variable mutation loads, suggesting that it is possible to obtain rats with higher mutation loads through genetic breeding.

Furthermore, we analyzed the phenotype of G007A, G1030A, and G11714/5A F_1 rats. The G007A F_1 rats showed impaired motor ability and a DCM phenotype. It has been reported that the mutation in mtDNA-encoded tRNA is an important genetic risk factor to cardiomyopathy.[14–16] However, the relationship between mt-tRNA mutations and disease development is complex and remains inconclusive, largely accounting for the shortage of mitochondrial disease animal models. Several groups have been reported that pathogenic mutations affect the efficiency of 3′ processing, aminoacylation, the stability of tRNA, the tertiary structure of tRNA, and interaction of tRNA with its partner molecular, which results in the decrease of translation efficiency of mtDNA-encoded proteins.[16–20] The deficiency of mtDNA-encoded proteins further leads to mitochondrial dysfunction along with ATP production decrease and reactive oxygen species (ROS) level increase.[21–24] In human $tRNA^{Phe}$, the G583A mutation (G007A in rat) resulted in significant losses in aminoacylation efficiency by hmt-PheRS, which could impair the translation of mtDNA-encoded proteins.[25] The G007A mutation results in tRNA metabolism impairment and further leads to the decrease of mitochondrial proteins and ATP production in rats. The heart is a constant mechanical pump that is dependent on continuous energy supply, which is mainly provided by mitochondrial OXPHOS. mtDNA mutations play a detrimental role on cardiac contractile function and therefore cause DCM.[26]

We did not observe disease phenotypes in G1030A rats, probably due to the low mutation loads (X.Q., and Y.M., unpublished data). For G11714/5A rats, although no motor ability was observed, the F_1 rats showed a HCM phenotype. However, the relationship between genotype and phenotype is complicated. Indeed, the same mutation results in different pathologies, while the same pathology can be correlated with different mutations. This might be explained by the heteroplasmy. In addition, the different usage rate of tRNA (Phe) and tRNA (Leu^{CUN}) in translation of 13 mtDNA coding genes might play a role for the different phenotype induced by G007A and G11714/5A mutations, respectively. It is important to decipher the underlying molecular and biochemical mechanisms linking any mutation in tRNA genes to the corresponding pathological phenotype. Our data might suggest that patients with the G12315/6A dual mutation might have a risk of HCM.

In addition, the off-target potential is the primary concern for all editing tools. We analyzed all possible mutations in the whole mitochondrial genome and nuclear genome, and the results showed that only limited off-target editing was detected. Two recently published papers showed that DdCBE mediated a high off-target effect in the nuclear genome in HEK293T cells and mice embryos.[27,28] Single-nucleotide variations (SNVs) are variable between SD rat individuals, even in the parent and their offspring. It is difficult to confirm that the variation in the nuclear genome comes from DdCBE-mediated off-target effects or just that SNVs derived from random mutations occur generation to generation. Here, we focus on the TALE sequence-dependent off-target analysis. In this study, 18 potential OTSs with sequences completely identical to their corresponding TALE sequences picked from the nuclear genome were analyzed, and no detectable off-target editing events were observed in the edited rats. This method probably misses the TALE sequence-independent OTSs. Indeed, a more precise off-target analysis tool needs to be developed. On the other hand, the off-target effect in the nuclear genome can be diluted by cross-breeding and might not be a significant concern for mtDNA mutant animals. Our results showed that the DdCBE established in this study could mediate precise base editing in a rat mtDNA aC context with limited off-target effects both on the mitochondrial genome and the nuclear genome.

In summary, for the first time, we established a particular combination of the DdCBE pair for rat mtDNA targeting at aC sites to resemble

Figure 3. G007A-edited rats show a DCM phenotype

(A) Sanger sequencing chromatograms of heart and skeletal muscle tissues of G007A F_0-#13 rat. (B) Mutation loads in G007A F_0-#13 heart, skeletal muscle, and toe. (C) H&E staining of heart and skeletal muscle tissues from G007A F_0-#13 and wild-type (WT) rats. Scale bar: 40 μm. (D) TEM images of mitochondria in G007A F_0-#13 heart and skeletal muscle tissues. (E) The protein levels of TOMM20 and mitochondrial respiratory chain complex subunits in heart and skeletal muscle tissue from G007A F_0-#13 and WT rats. (F) Screenshot of M-mode echocardiography for G007A F_1 and WT rats. (G–K) The cardiac structure and function parameters of WT and G007A F_1 rats calculated from echocardiography. Left ventricular (LV) the diameter at end of systole (LVIDS) (G) and diastole (LVIDD) (H); LV volume at the end of systole (LVVS) (I) and diastole (LVVD) (J); and LV ejection fraction (LVEF) (K). (L) The distance moved of WT and G007A F_1 rats in the OFT. (G–L) n = 10 for each group, quantitative data were analyzed with the two-tailed unpaired Student's t test and are presented as mean ± SEM. *$p \leq 0.05$; **$p \leq 0.01$.

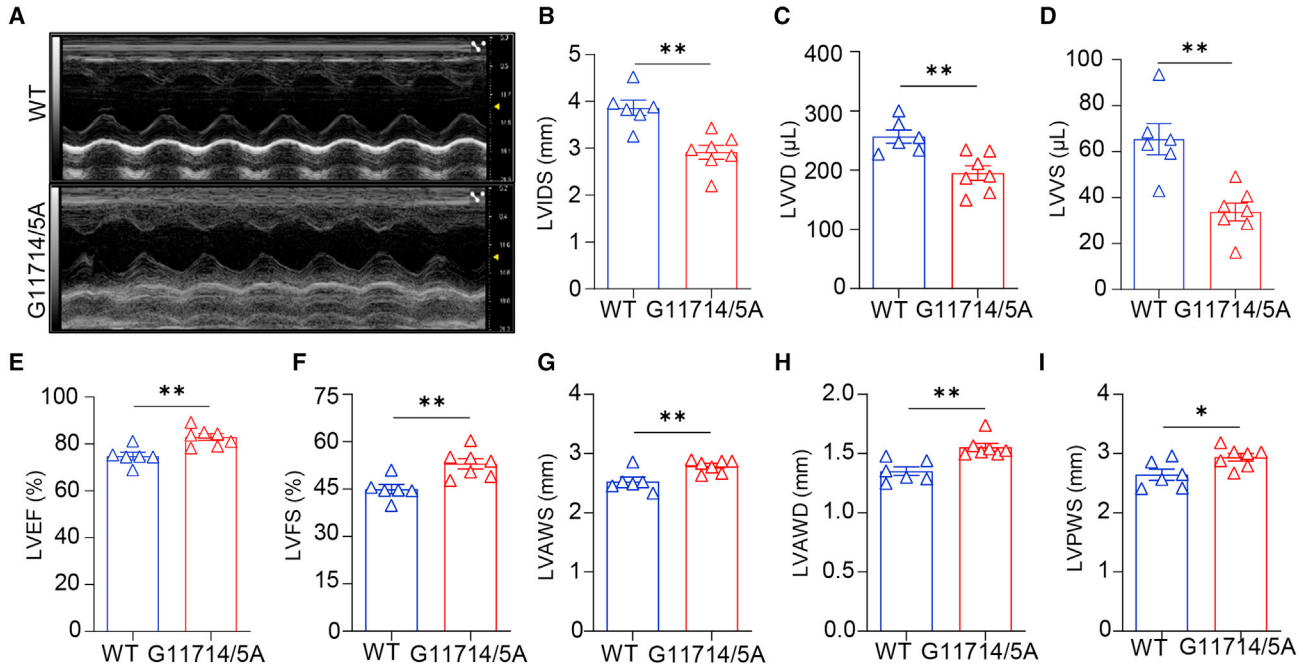

Figure 4. G11714/5A-edited rats display an HCM phenotype

(A) Screenshot of M-mode echocardiography for G11714/5A F_1 and WT rats. (B–I) The cardiac structure and function parameters of G11714/5A F_1 and WT rats calculated from echocardiography. LVIDS (B); LVVD (C) and LVVS (D); LVEF (E); LV percentage fractional shortening (LVFS) (F); LV anterior wall thickness at end of systole (LVAWS) (G) and diastole (LVAWD) (H); and LV posterior wall thickness at end of systole (LVPWS) (I). (B–I) n = 6 for WT and n = 7 for G11714/5A, quantitative data were analyzed with the two-tailed unpaired Student's t test and are presented as mean ± SEM. *$p \leq 0.05$; **$p \leq 0.01$.

human mitochondrial diseases. Moreover, the mutant rats exhibited distinct signs of cardiomyopathy, which provides a valuable disease model for the pathological process study of mitochondrial disorders. Although limited off-target effects were observed, more precise mtDNA editing tools should be developed to install pathogenic mtDNA mutations in animal models to study mitochondrial disease and to serve future gene therapeutic purposes.

MATERIALS AND METHODS

DdCBE expression plasmids construction

The DdCBE targeting plasmids were assembled using the Golden Gate strategy with an RVD library described before.[2,3] The assembled plasmids were confirmed by Sanger sequencing using RVD seq Fwd and RVD seq Rev primers (Tables S3 and S4). To construct the PB-DdCBE expression plasmids, the DdCBE coding sequence was cloned into pCAG-T7-MTS vector by using *Not* I and *Pme* I double enzyme digestion.

Cell culture and nucleofection

Rat glioma C6 cells (ATCC, CCL-107) were cultured in DMEM supplemented with 10% FBS at 37°C with 5% CO_2 and were detected without mycoplasma contamination by PCR test. Cells were co-transfected with 400 ng left-DdCBE and 400 ng right-DdCBE using Lonza 4D-Nucleofector by SF Cell Line 4D-Nucleofector X Kit. Cells were supplemented with 0.6 μg/mL puromycin 24 h post nucleofection and collected at day 3 for DNA extraction.

Animals

The SD rats used in this study were purchased from Beijing Vital River Laboratories Animal Technology and housed in an AAALAC-accredited standard facility. All animal procedures and experiments were approved by the Institutional Animal Care and Use Committee (IACUC) of the Institute of Laboratory Animal Science, Chinese Academy of Medical Sciences & Peking Union Medical College (IACUC-MYW21006). All mutant rats established in this study were preserved at the Rat Resource Center of China (www.ratresource.com).

Microinjection of rat fertilized eggs

The fertilized rat eggs were collected and microinjected following the procedure described previously.[11] In brief, 4- to 6-week-old female rats were intraperitoneally (i.p.) injected with pregnant mare serum gonadotropin (PMSG; Sigma-Aldrich) and human chorionic gonadotropin (hCG; Sigma-Aldrich). After hCG injection, the female rats were immediately mated with male rats. On the next morning, 1-cell embryos were collected from superovulated female rats and cultured in KSOM (Millipore) at 37°C and 5% CO_2. The purified PB-DdCBE pair with a concentration of 14 ng/μL was injected into the cytoplasm of zygotes using a Nikon microinjection system following the instructions. The injected zygotes were transferred to pseudopregnant SD rats.

DNA extraction and genotyping

Genomic DNA and mitochondria genome of C6 cells were extracted using QuickExtract DNA Extraction Solution (Lucigen). Genomic

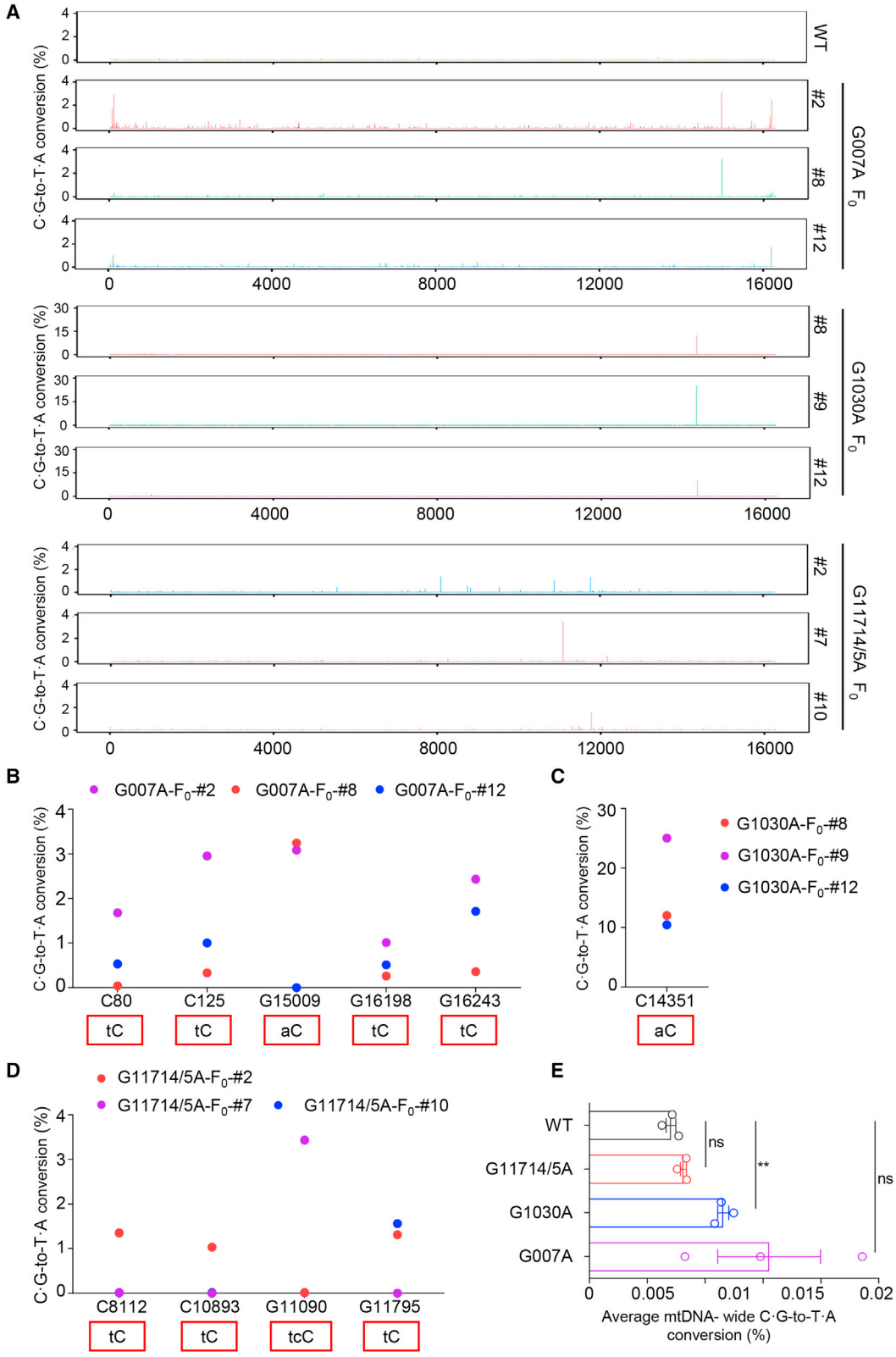

(legend on next page)

DNA and mitochondria genome of rat tissues were extracted using the EasyPure Genomic DNA Kit (EE101, TransGen) or the QIAamp@DNA Micro Kit (56304, Qiagen) after proteinase K digestion. The target sites were amplified and further confirmed by Sanger sequencing. The primers are listed in Table S3.

Echocardiography analysis

Heart structure and function were evaluated by echocardiography analysis as described previously.[3] In brief, the rats were anesthetized with isoflurane, and echocardiographic observation was performed using a Vevo3100 ultrasound machine with an MX201 probe (15 MHz) following the instructions (VisualSonics, Fujifilm). Measurements were recorded for at least three continuous cardiac cycles.

Open field test (OFT)

OFT was performed in an 80 × 80 × 50 cm black box. Rat spontaneous behavior was recorded for 5 min using a SuperMaze digital tracking system (v.2.1, Shanghai Xinruan Informatlon Technology, Shanghai, China). All tracks were analyzed using a SuperMaze software.

ATP measurement

The ATP levels in heart and muscle tissues were measured by an ATP Colorimetric Assay Kit (K354-100, BioVision). In brief, 20 mg fresh tissue was homogenized in 200 μL ATP assay buffer, followed by deproteinization using a ReadiUse TCA Deproteinization Sample Preparation Kit (19501, AAT Bioquest). Fifty μL prepared sample and ATP standards were added to a 96-well plate, and the volume was adjusted to 50 μL/well using ATP assay buffer. Then, 50 μL reaction mix (44 μL ATP assay buffer, 2 μL ATP probe, 2 μL ATP converter, and 2 μL developer) was added to each well. After incubation at room temperature for 30 min, a microplate reader (Multiskan FC with Incubator 51119100, Thermo Fisher Scientific) was used to measure the light absorption value (OD 570 nm). The ATP level was calculated based on the standard curve.

H&E staining

Tissues collected from rats were fixed in 4% buffered formalin solution and prepared paraffin sections at 3–4 μm. After dewaxing, all the tissue sections were stained with H&E according to methods described previously.[29] H&E-stained slides were scanned with CaseViewer software (3DHISTECH, Budapest, Hungary).

TEM

TEM was carried out as previously described.[29] Briefly, fresh cardiac muscle and skeleton muscle were fixed in 2.5% glutaraldehyde after perfusion with ice-cold PBS. Then, the fixed tissues were steeped in 1% osmium tetroxide for 2 h. Following dehydration with a serial alcohol gradient, samples were embedded in Epon812 resin, sectioned into approximately 90 nm slices, and then stained with uranyl acetate and lead citrate. The slices were observed using TEM (JEM-1400, JEOL, Tokyo, Japan).

Western blot

Total proteins of tissues were extracted using radioimmunoprecipitation assay (RIPA) lysis buffer supplemented with protease inhibitor cocktail and PMSF. Proteins were separated by 10% or 12% SDS-PAGE following standard procedures after quantification with a BCA protein assay kit (P0012S, Beyotime, Shanghai, China). The primary antibodies anti-ND1 (Proteintech 19703-1-AP; 1:1,000); anti-NDUFA9 (Abcam ab14713; 1:1,000); anti-SDHB (Abcam ab14714; 1:200); anti-CYB (Proteintech 55090-1-AP; 1:1,000); anti-UQCRC2 (Abcam ab14745; 1:1,000); anti-ATP8 (ABclonal A17890, 1:1,000); anti-ATP5A (Abcam ab176569; 1:1,000); anti-COX IV (Proteintech 11242-1-AP; 1:1,000); anti-MT-CO3 (Proteintech 55082-1-AP; 1:500); anti-TOMM20 (Proteintech 11802-1-AP; 1:2,000); and anti-β actin (Abcam ab8227; 1:5,000) were used. HRP-conjugated secondary antibodies (ZSGB-BIO) were diluted 1:5,000. Protein signals were detected using an enhanced enhanced chemiluminescence (ECL) western blot substrate (P0018S, Beyotime) and visualized by a Bio-Rad imaging system.

Mitochondrial mRNA level detection

The total mRNA of heart and muscle tissue was extracted using TRIzol reagent (Thermo Fisher Scientific) following the manufacturer's instructions. The purity and quantity of RNA were evaluated with the NanoDrop 2000 (Thermo Fisher Scientific). The cDNAs were synthesized using the EasyScript All-in-One First-Strand cDNA Synthesis SuperMix (AE341, TransGen). Real-time PCR was carried out using TransStart Top Green qPCR SuperMix (AQ132, TransGen). Primers used for rat mitochondrial transcript detection are listed in Table S3. Transcript quantities were normalized to β-actin as reference control.

Analyze mtDNA copy number

The mtDNA copy number was assessed by real-time quantitative PCR using Sequence Detection System (QuantStudio 3, Applied Biosystems, Waltham, MA, USA) and TransStart Top Green qPCR SuperMix (AQ132, TransGen) according to a precious report.[30] The primers used for mtDNA copy-number analysis are listed in Table S3.

Deep sequencing

The target region was first amplified with barcoded primers (first round PCR [PCR1]) using Phanta Max Super-Fidelity DNA Polymerase (P505, Vazyme). Then, the PCR1 products were pooled with equal

Figure 5. Off-target analysis of the whole mitochondria genome

(A) Off-target effects were analyzed on the whole mitochondrial genome in G007A, G1030A, and G11714/5A F_0 rats. WT rat (top lane) was used as controls. (B–D) Off-target sites with over 1% editing efficiency were further analyzed in G007A F_0 rats (B), G1030A F_0 rats (C), and G11714/5A F_0 rats (D). The motifs of off-target sites are shown at bottom. (E) Average frequency of mitochondria genome-wide C• G-to-T •A conversions for F_0 rat. (E) Quantitative data were analyzed with the two-tailed unpaired Student's t test and are presented as mean ± SEM. ns, not significant; *$p \leq 0.05$ (n = 3 for each group).

moles and purified for the second round of PCR (PCR2). PCR2 was performed using index primers (N321/N322, Vazyme) and purified using DNA Clean Beads (N411, Vazyme). Sequencing was performed using the Illumina NovaSeq platform. The barcoded primers used for PCR1 are listed in Table S3.

Whole mtDNA sequencing

Two overlapping fragments of approximately 8 kb each were amplified using primers for long-range PCR and purified by gel extraction. The two fragments were pooled with equal moles and subjected to library preparation using TruePrep DNA Library Prep Kit V2 for Illumina (TD501, Vazyme). The libraries were purified using DNA Clean Beads by 0.5/0.3× double size selection. Libraries were pooled and sequenced by the Illumina NovaSeq platform. The primers used for amplification of long-range PCR are listed in Table S3.

Off-target analysis

The off-target effects were analyzed in whole mitochondrial genome and nuclear genome. For nuclear DNA off-target analysis, the sequences from rat nuclear genome (assembly mRatBN7.2) identical to each TALE binding site were selected and amplified to perform deep sequencing for off-target analysis. The primers used for deep sequencing are listed in Table S3. The off-target effects in mitochondrial genome were analyzed by whole mtDNA sequencing.

Data analysis

To calculate the editing frequency, the sequencing reads were trimmed by Trim Galore in paired-end mode and were aligned to the mitochondrial genome reference sequence of *Rattus norvegicus* (NC_001665) using bowtie2 with default parameters of paired end. Then, the alignment results were converted to bam format by Samtools. Samtools mpileup was used to detect C-to-T or G-to-A conversion for DdCBE-mediated editing. The SNP sites were excluded before analysis according to the following criteria: (1) SNP sites of *Rattus norvegicus* were obtained from variation VCF in the Ensembl database, and (2) the sites with over 1% C•G-to-T•A conversion in any untreated sample.

To calculate the mitochondrial genome-wide average off-target editing frequency, the editing events within spacing regions were excluded. The sites were excluded before analysis according to the following criteria: (1) SNP sites of *Rattus norvegicus* were obtained from variation VCF in Ensembl database; (2) the sites with over 1% C•G-to-T•A conversion in any untreated sample; (3) the sites with over 90% C•G-to-T•A conversion in any sample; and (4) the sites within the DdCBE spacing region. The average off-target editing frequency was then calculated independently for each biological replicate as follows: (number of reads in which a given C•G base pair was called as a T•A base pair, summed over all non-target C•G base pairs)/(total number of reads that covered all non-target C•G base pairs).

To calcualte the off-target editing in nuclear genome, 20 bp sequences downstream of the TALE recognition site were analyzed to detect C•G-to-T•A conversion. Targeted deep sequencing was carried out at a sequencing depth of >8,000×, and mutations with over 0.2% editing were regardes as off-target events.

Statistical analysis

The data from the deep sequencing, echocardiography analysis, OFT, ATP measurements, and complex activity assays were analyzed using Prism 8 (GraphPad). Data were represented as mean ± SEM. p values were calculated using a two-tailed unpaired Student's t test. ns, not significant; *$p \leq 0.05$; **$p \leq 0.01$; ***$p \leq 0.001$; ****$p \leq 0.0001$.

DATA AVAILABILITY

The high-throughput sequencing data from this study have been deposited in the NCBI Sequence Read Archive (SRA) database (NCBI: PRJNA851525).

SUPPLEMENTAL INFORMATION

Supplemental information can be found online at https://doi.org/10.1016/j.omtn.2023.02.028.

ACKNOWLEDGMENTS

This work was supported by the National Key Research and Development Program of China (2021YFC2700600), the Funds for Creative Research Groups of China (82221005), the National Natural Science Foundation of China (31970796), the CAMS Innovation Fund for Medical Sciences of China (CIFMS, 2021-I2M-1-024, 2021-I2M-1-034, and 2021-1-I2M-018), the Beijing Municipal Natural Science Foundation (Grant No. M21004), the Beijing Nova Program (Z211100002121034), the Leading Talents of Guangdong province program (2016LJ06S386), and the 111 Project of Ministry of Education (B20095).

AUTHOR CONTRIBUTIONS

Y.M. and B.S. conceived the project and designed the experiments. X.Q., X.Z., W.C., W.K., W.D., L.L., L.G., D.L., J.G., F.G., X.H., L.Z., and Y.M. performed microinjections, breeding, rat sample collection, mutation analysis, behavior analysis, western blot, and ATP level detection of rat. L.T. and J.W. performed all plasmid construction, sequencing, and cell culture. J.J., W.S., and S.W. performed the computational analyses. X.Q., Y.M., and B.S. wrote the manuscript with input from all authors.

DECLARATION OF INTERESTS

The authors declare no competing interests.

REFERENCES

1. Stewart, J.B. (2021). Current progress with mammalian models of mitochondrial DNA disease. J. Inherit. Metab. Dis. *44*, 325–342.

2. Guo, J., Zhang, X., Chen, X., Sun, H., Dai, Y., Wang, J., Qian, X., Tan, L., Lou, X., and Shen, B. (2021). Precision modeling of mitochondrial diseases in zebrafish via DdCBE-mediated mtDNA base editing. Cell Discov. *7*, 78.

3. Qi, X., Chen, X., Guo, J., Zhang, X., Sun, H., Wang, J., Qian, X., Li, B., Tan, L., Yu, L., et al. (2021). Precision modeling of mitochondrial disease in rats via DdCBE-mediated mtDNA editing. Cell Discov. *7*, 95.

4. Mok, B.Y., Kotrys, A.V., Raguram, A., Huang, T.P., Mootha, V.K., and Liu, D.R. (2022). CRISPR-free base editors with enhanced activity and expanded targeting scope in mitochondrial and nuclear DNA. Nat. Biotechnol. *40*, 1378–1387.
5. Hanna, M.G., Nelson, I.P., Morgan-Hughes, J.A., and Wood, N.W. (1998). MELAS: a new disease associated mitochondrial DNA mutation and evidence for further genetic heterogeneity. J. Neurol. Neurosurg. Psychiatry *65*, 512–517.
6. Darin, N., Kollberg, G., Moslemi, A.R., Tulinius, M., Holme, E., Grönlund, M.A., Andersson, S., and Oldfors, A. (2006). Mitochondrial myopathy with exercise intolerance and retinal dystrophy in a sporadic patient with a G583A mutation in the mt tRNA(phe) gene. Neuromuscul. Disord. *16*, 504–506.
7. Sacconi, S., Salviati, L., Gooch, C., Bonilla, E., Shanske, S., and DiMauro, S. (2002). Complex neurologic syndrome associated with the G1606A mutation of mitochondrial DNA. Arch. Neurol. *59*, 1013–1015.
8. Mansour, H.A., Chacko, J.A., Sanders, R.N., Schaefer, G.B., and Uwaydat, S.H. (2022). Retinal degeneration associated with the G1606A mitochondrial mutation. Ophthalmic Surg. Lasers Imaging Retina *53*, 116–119.
9. Sazonova, M.A., Sinyov, V.V., Barinova, V.A., Ryzhkova, A.I., Zhelankin, A.V., Postnov, A.Y., Sobenin, I.A., Bobryshev, Y.V., and Orekhov, A.N. (2015). Mosaicism of mitochondrial genetic variation in atherosclerotic lesions of the human aorta. BioMed Res. Int. *2015*, 825468.
10. Sobenin, I.A., Sazonova, M.A., Postnov, A.Y., Salonen, J.T., Bobryshev, Y.V., and Orekhov, A.N. (2013). Association of mitochondrial genetic variation with carotid atherosclerosis. PLoS One *8*, e68070.
11. Ma, Y., Zhang, X., Shen, B., Lu, Y., Chen, W., Ma, J., Bai, L., Huang, X., and Zhang, L. (2014). Generating rats with conditional alleles using CRISPR/Cas9. Cell Res. *24*, 122–125.
12. Karadimas, C.L., Salviati, L., Sacconi, S., Chronopoulou, P., Shanske, S., Bonilla, E., De Vivo, D.C., and DiMauro, S. (2002). Mitochondrial myopathy and ophthalmoplegia in a sporadic patient with the G12315A mutation in mitochondrial DNA. Neuromuscul. Disord. *12*, 865–868.
13. Ronchi, D., Virgilio, R., Bordoni, A., Fassone, E., Sciacco, M., Ciscato, P., Moggio, M., Govoni, A., Corti, S., Bresolin, N., and Comi, G.P. (2010). The m.12316G>A mutation in the mitochondrial tRNA Leu(CUN) gene is associated with mitochondrial myopathy and respiratory impairment. J. Neurol. Sci. *292*, 107–110.
14. Campbell, T., Slone, J., and Huang, T. (2022). Mitochondrial genome variants as a cause of mitochondrial cardiomyopathy. Cells *11*, 2835.
15. Bayona-Bafaluy, M.P., Iglesias, E., López-Gallardo, E., Emperador, S., Pacheu-Grau, D., Labarta, L., Montoya, J., and Ruiz-Pesini, E. (2020). Genetic aspects of the oxidative phosphorylation dysfunction in dilated cardiomyopathy. Mutat. Res. Rev. Mutat. Res. *786*, 108334.
16. Florentz, C., Sohm, B., Tryoen-Tóth, P., Pütz, J., and Sissler, M. (2003). Human mitochondrial tRNAs in health and disease. Cell. Mol. Life Sci. *60*, 1356–1375.
17. Suzuki, T., Nagao, A., and Suzuki, T. (2011). Human mitochondrial tRNAs: biogenesis, function, structural aspects, and diseases. Annu. Rev. Genet. *45*, 299–329.
18. Meng, F., Jia, Z., Zheng, J., Ji, Y., Wang, J., Xiao, Y., Fu, Y., Wang, M., Ling, F., and Guan, M.X. (2022). A deafness-associated mitochondrial DNA mutation caused pleiotropic effects on DNA replication and tRNA metabolism. Nucleic Acids Res. *50*, 9453–9469.
19. Yasukawa, T., Suzuki, T., Ishii, N., Ohta, S., and Watanabe, K. (2001). Wobble modification defect in tRNA disturbs codon-anticodon interaction in a mitochondrial disease. EMBO J. *20*, 4794–4802.
20. Chomyn, A., Enriquez, J.A., Micol, V., Fernandez-Silva, P., and Attardi, G. (2000). The mitochondrial myopathy, encephalopathy, lactic acidosis, and stroke-like episode syndrome-associated human mitochondrial tRNALeu(UUR) mutation causes aminoacylation deficiency and concomitant reduced association of mRNA with ribosomes. J. Biol. Chem. *275*, 19198–19209.
21. Liu, Y., and Chen, Y. (2020). Mitochondrial tRNA mutations associated with essential hypertension: from molecular genetics to function. Front. Cell Dev. Biol. *8*, 634137.
22. Richter, U., McFarland, R., Taylor, R.W., and Pickett, S.J. (2021). The molecular pathology of pathogenic mitochondrial tRNA variants. FEBS Lett. *595*, 1003–1024.
23. Ding, Y., Gao, B.B., and Huang, J.Y. (2020). The role of mitochondrial DNA mutations in coronary heart disease. Eur. Rev. Med. Pharmacol. Sci. *24*, 8502–8509.
24. Hahn, A., and Zuryn, S. (2019). Mitochondrial genome (mtDNA) mutations that generate reactive oxygen species. Antioxidants *8*, 392.
25. Ling, J., Roy, H., Qin, D., Rubio, M.A.T., Alfonzo, J.D., Fredrick, K., and Ibba, M. (2007). Pathogenic mechanism of a human mitochondrial tRNAPhe mutation associated with myoclonic epilepsy with ragged red fibers syndrome. Proc. Natl. Acad. Sci. USA *104*, 15299–15304.
26. Murphy, E., Ardehali, H., Balaban, R.S., DiLisa, F., Dorn, G.W., 2nd, Kitsis, R.N., Otsu, K., Ping, P., Rizzuto, R., Sack, M.N., et al. (2016). Mitochondrial function, biology, and role in disease: a scientific statement from the American heart association. Circ. Res. *118*, 1960–1991.
27. Wei, Y., Li, Z., Xu, K., Feng, H., Xie, L., Li, D., Zuo, Z., Zhang, M., Xu, C., Yang, H., and Zuo, E. (2022). Mitochondrial base editor DdCBE causes substantial DNA off-target editing in nuclear genome of embryos. Cell Discov. *8*, 27.
28. Guo, J., Chen, X., Liu, Z., Sun, H., Zhou, Y., Dai, Y., Ma, Y., He, L., Qian, X., Wang, J., et al. (2022). DdCBE mediates efficient and inheritable modifications in mouse mitochondrial genome. Mol. Ther. Nucleic Acids *27*, 73–80.
29. Ling, Y., Yang, X., Zhang, X., Guan, F., Qi, X., Dong, W., Liu, M., Ma, J., Jiang, X., Gao, K., et al. (2022). Myocardium-specific Isca1 knockout causes iron metabolism disorder and myocardial oncosis in rat. Life Sci. *297*, 120485.
30. Silva Ramos, E., Motori, E., Brüser, C., Kühl, I., Yeroslaviz, A., Ruzzenente, B., Kauppila, J.H.K., Busch, J.D., Hultenby, K., Habermann, B.H., et al. (2019). Mitochondrial fusion is required for regulation of mitochondrial DNA replication. PLoS Genet. *15*, e1008085.